NANO LETTERS

Letter

pubs.acs.org/NanoLett

Chemical Vapor Deposition and Characterization of Aligned and Incommensurate Graphene/Hexagonal Boron Nitride Heterostack on Cu(111)

Silvan Roth,*[,†] Fumihiko Matsui,[‡] Thomas Greber,[†] and Jürg Osterwalder[†]

[†]Physik-Institut, Universität Zürich, Winterthurerstrasse 190, CH-8057 Zürich, Switzerland

[‡]Graduate School of Materials Science, Nara Institute of Science and Technology (NAIST), Ikoma, Nara 630-0192, Japan

ABSTRACT: Two limiting factors for a new technology of graphene-based electronic devices are the difficulty of growing large areas of defect-free material and the integration of graphene with an atomically flat and insulating substrate material. Chemical vapor deposition (CVD) on metal surfaces, in particular on copper, may offer a solution to the first problem, while hexagonal boron nitride (h-BN) has been identified as an ideal insulating substrate material. The bottom-up growth of graphene/h-BN stacks on copper surfaces appears therefore as a promising route for future device fabrication. As an important step, we demonstrate the consecutive growth of well-aligned graphene on h-BN, both as single layers, by low-pressure CVD on Cu(111) in an ultrahigh vacuum environment. The resulting films show a largely predominant orientation, defined by the substrate, where the graphene lattice aligns parallel to the h-BN lattice, while each layer maintains its own lattice constant. The lattice mismatch of 1.6% between h-BN and graphene leads to a moiré pattern with a periodicity of about 9 nm, as observed with scanning tunneling microscopy. Accordingly, angle-resolved photoemission data reveal two slightly different Brillouin zones for electronic states localized in graphene and in h-BN, reflecting the vertical decoupling of the two layers. The graphene appears n-doped and shows no gap opening at the $\bar{K}$ point of the two-dimensional Brillouin zone.

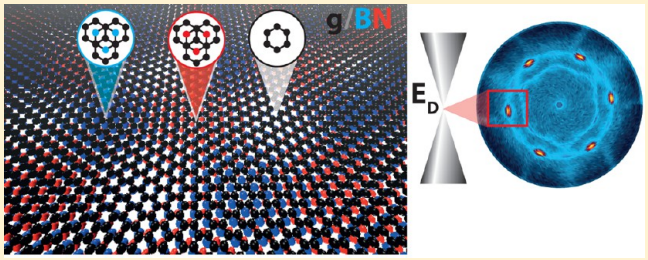

KEYWORDS: *Graphene, hexagonal boron nitride, chemical vapor deposition, heterostack, moiré pattern*

Graphene is a single-layer sp^2 hybridized honeycomb carbon network, which shows outstanding stability, crystalline perfection, and electronic properties. Using single graphene sheets exfoliated from graphite samples, a great potential for applications in future electronics has been demonstrated in recent years.[1] However, samples produced in this way are tiny and have to be transferred onto a suitable insulating substrate for device fabrication. Therefore the method can hardly be upscaled. Moreover, key properties, like the electron mobility[2] or the long ballistic mean free path,[3] are limited by the structural and electronic roughness of the substrate.[4,5]

Two different routes have so far been followed in order to upscale the production of single-layer graphene. Controlled graphitisation of Si-terminated SiC(0001) in an argon atmosphere of 1 bar was shown to produce graphene layers on the wafer scale with relatively large domain sizes and good mobilities.[6] The second route involves large-area synthesis of single-layer graphene films on copper foils[7,8] by chemical vapor deposition (CVD), which is self-terminating at the single-layer stage due to the catalytic involvement of the metal surface. The method has been extended soon after to the direct roll-to-roll production of 30 in. graphene films for transparent electrodes.[9] In order to exploit the unique properties of the graphene layers, the copper foil or thin film has to be etched away by chemical means, and the graphene layer needs to be transferred onto an insulating substrate. The polycrystalline nature of the copper substrates limits the structurally coherent domain size within the graphene monolayer.

Hexagonal boron nitride (h-BN) has been a natural candidate substrate for graphene-based electronic devices, due to its insulating nature and close structural relationship.[10,11] Its individual layers exhibit the same honeycomb network, here heteroatomic, with a lattice mismatch of 1.6%,[12,13] and the material has a large energy gap of about 6 eV.[14] Indeed, by building devices using exfoliation techniques, it could be shown that graphene on h-BN exhibits the best electronic properties demonstrated so far.[15] Consequently, various groups have explored the consecutive epitaxial growth of graphene on h-BN. Already in the year 1996, the Oshima group reported the heteroepitaxial growth of monolayer graphene on monolayer h-BN on Ni(111).[16−18] Their two-step low-pressure CVD growth method involved high-temperature exposure of the atomically clean nickel surface to benzene-like borazine $(HBNH)_3$ to form the h-BN layer and subsequent much higher exposure to benzene in order to grow the graphene layer. The characterization of these films by low-energy electron diffraction

Received: March 5, 2013
Revised: May 6, 2013
Published: May 9, 2013

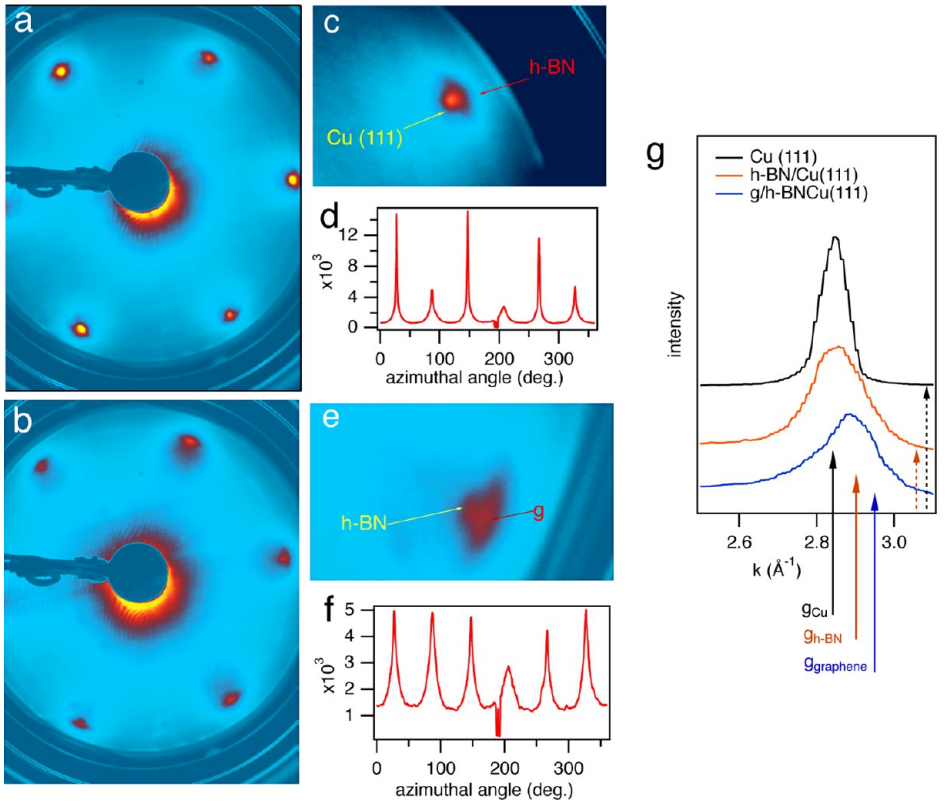

Figure 1. Layer orientation. LEED patterns at an electron energy of 70 eV taken from a single layer of h-BN on Cu(111) (a) and from a single-layer g/h-BN/Cu(111) stack (b). Panel (c) zooms in to a principal spot of (a), while (e) zooms in to a spot in (b), showing the contributions from substrate and h-BN layer, and from the g/h-BN stack, respectively. (d,f) Intensity distributions along circular paths in (a) and (b), respectively, containing all six principal spots. (g) Radial cuts through the LEED spots for each preparation stage (offsets indicated).

(LEED) showed that most parts of the surface are covered with graphene flakes with their lattices oriented in the same way as the underlying h-BN layer, while other rotated domains are present as a minority species. Scanning tunneling microscopy (STM) images showed atomic corrugations that were vaguely interpreted in terms of two incommensurate layers[18] but were not more conclusive. More recently, a similar system was studied by angle-resolved photoemission spectroscopy (ARPES).[19] Here, the low-pressure CVD growth of the graphene layer was preceded by an extra step in which Au atoms were intercalated between the h-BN monolayer and the Ni(111) surface. This resulted in an effective decoupling of the double layer from the substrate, confirmed by the appearance of a gapless and linearly dispersing graphene π-band within the h-BN band gap, passing through the Fermi level near the $\bar{K}$ point of the two-dimensional Brillouin zone. Further studies included the single-layer g/h-BN growth on Ru(0001),[20] as well as large-area growth of few-layer g/h-BN stacks on graphite or copper foils.[21] In both cases the typical Raman signature of graphene was demonstrated.

In all previous studies of g/h-BN heterogrowth, there was no conclusive structural characterization of the double layer, nor how the structural relationship is reflected in the electronic bands. The structural issue has been addressed in a recent study by the group of LeRoy by using exfoliated samples of graphene and h-BN in order to form the double layer.[22] STM images showed very flat surfaces and the appearance of different moiré patterns, depending on the relative orientation of the individual graphene and h-BN flakes. In this Letter, we demonstrate the growth of well-aligned g/h-BN double layers by two-step low-pressure CVD on Cu(111) and use X-ray photoelectron diffraction (XPD), LEED, and STM for structural analysis as well as ARPES for a precise characterization of the electronic structure.

The exposure of the hot Cu(111) surface (T = 1050 K) to borazine ($p = 5 \times 10^{-6}$ mbar) results in the formation of a single h-BN layer.[23,24] The orientation of this layer is guided by the Cu surface during the growth procedure. As a consequence, the h-BN lattice is oriented almost parallel to the surface lattice of the substrate. The LEED pattern in Figure 1a shows the hexagonal arrangement of six principal diffraction spots with the 3-fold symmetry of the Cu(111) surface still reflected in the spot intensities (see also intensity distribution in Figure 1d). A closer look at the LEED spots (Figure 1c) reveals a slight difference for the in-plane reciprocal lattice vectors $g_{(BN)}$ and $g_{(Cu)}$. The difference of 1.9 ± 0.1% agrees well with a lattice mismatch of 1.8% found for this system in a recent low-temperature STM study based on the analysis of moiré patterns.[24] Figure 1c further indicates that the h-BN lattice is not aligned precisely with the Cu(111) lattice but that there is a small angular spread (fwhm = 2.5°). Again, this confirms the results by Joshi et al.[24] where all observed moiré patterns could be reproduced with a relative angular spread of 3°.

The h-BN layer is stable up to high temperatures,[25] which allows the consecutive CVD growth of a graphene layer on top. Upon exposure of the h-BN/Cu(111) surface to 3-pentanone at a temperature of 1100 K and a pressure of p = 2.2 mbar, the principal diffraction spots in the LEED pattern persist, indicating the formation of a graphene layer that is predominantly aligned with the underlying h-BN layer (Figure

dx.doi.org/10.1021/nl400815w | Nano Lett. 2013, 13, 2668−2675

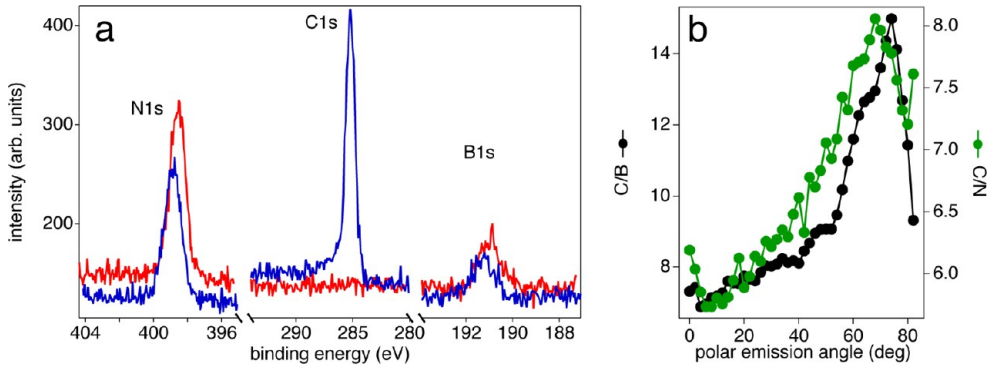

Figure 2. Single-layer characterization and stacking order. (a) Al Kα excited XPS normal emission spectra of nitrogen, carbon, and boron 1s core levels from the single-layer h-BN/Cu(111) system (red) and the single-layer g/h-BN/Cu(111) stack (blue). Intensities of different core levels are to scale with arbitrary offsets. (b) Ratios of C 1s to B 1s intensities (black) and C 1s to N 1s intensities (green) as a function of polar emission angle.

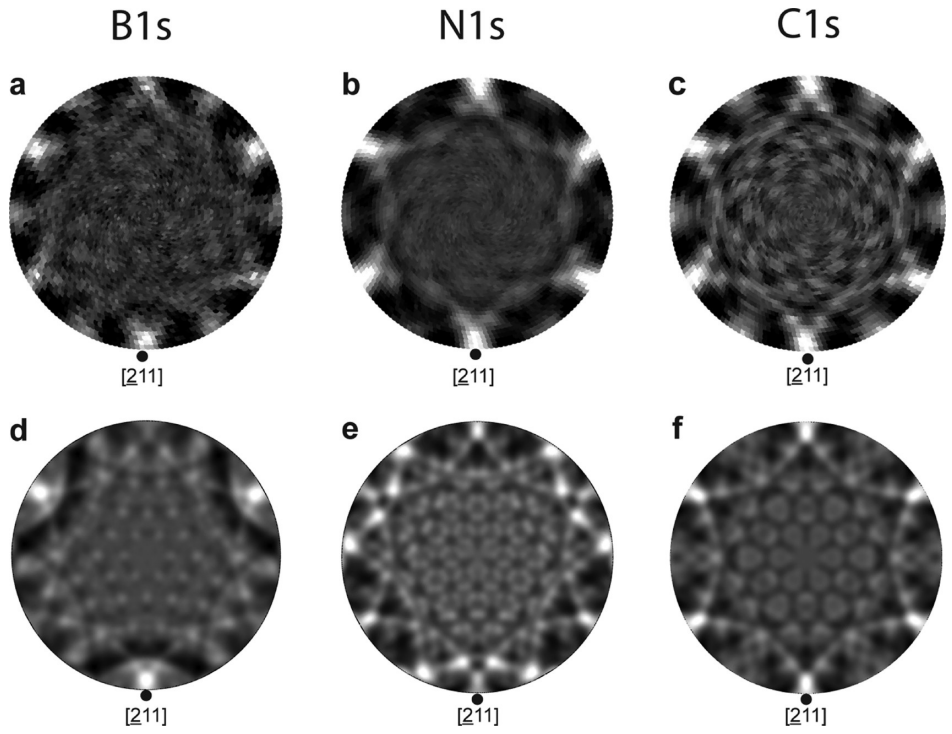

Figure 3. X-ray photoelectron diffraction. Stereographic representation of experimental (top row) and theoretical (bottom row) photoelectron diffraction patterns of B 1s, N 1s, and C 1s core levels, displayed in a linear gray scale for polar emission angles between 0 and 82°. The experimental data are taken from a g/h-BN/Cu(111) stack, while the MSC calculations were performed with a free-standing h-BN layer and a free-standing graphene layer, respectively, containing 120 atoms each.

1b). The spot intensities show here a 6-fold symmetry, that is, the substrate no longer influences the diffraction (see also intensity distribution shown in Figure 1f). The spots have become significantly broader (fwhm = 10°) with a concomitant increase of diffuse scattering. A weak ring of intensity is observed along a circle containing all principal spots, indicating the presence of a small area fraction of randomly rotated domains. This is in accordance with the results of Kawasaki et al.,[18] but the contribution of a distinct phase rotated by 30°, which was observed in their work, is very small in our data. The relative intensity of the ring with respect to the principal spots depends strongly on the preparation parameters. Lower substrate temperatures during the growth process consistently led to highly disoriented growth of the h-BN and the graphene layers (data not shown).

The single-layer character and the stacking order of the h-BN and graphene layers are established by X-ray photoelectron spectroscopy (XPS). Spectra of the 1s core levels of boron, nitrogen, and carbon are shown in Figure 2a. For the preformed h-BN layer the coverage is determined by comparing the B 1s and the N 1s intensities to that of the Cu 2p core level of the substrate. The coverage values obtained from B 1s (1.16 ML) and from N 1s (1.05 ML), using theoretical cross section values[26] and an electron inelastic mean free path of 16.9 Å[27] for the substrate photoelectrons, are consistent with a nearly stoichiometric and self-terminated growth of a single h-BN layer.

For the subsequent growth of the graphene layer, the catalytic activity of the bare metal surface is absent.[7,28] The CVD process therefore requires much higher precursor pressures, and reaching single-layer coverage needs to be

dx.doi.org/10.1021/nl400815w | Nano Lett. 2013, 13, 2668−2675

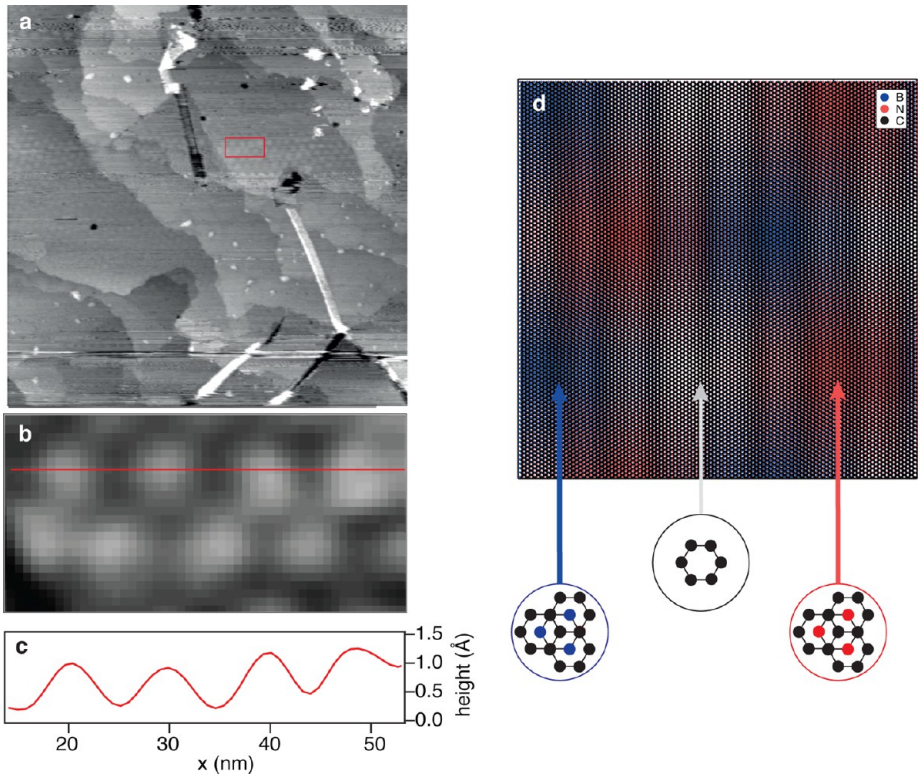

Figure 4. Large scale moiré pattern formation. (a) STM topographic image of graphene grown on h-BN/Cu(111) (400 × 400 nm). The imaging parameters are $V_t = -1.0$ V and $I_t = 0.1$ nA. (b) A zoom into the moiré pattern observed in (a) with the according height profile along the red line given in (c). (d) Visualization of a moiré pattern resulting from the superposition of a graphene layer (black) with a lattice constant of 2.46 Å and a h-BN layer (B red, N blue) with a lattice constant of 2.50 Å with the two lattice orientations fully aligned. The regions appearing blue result from C atoms covering B atoms, while in the red regions C atoms are on top of N atoms (see circular insets). In the black and white regions, the carbon atoms are on top of B and N atoms.

controlled via pressure, substrate temperature, and exposure time. For the films discussed in this work, the preparation temperature was chosen at 40 K higher than for graphene growth using 3-pentanone on Rh(111) (T = 1060 K).[29] In order to clarify the stacking order of the two layers, core level intensities were measured as a function of polar emission angle. The photoemission intensity ratios of C 1s/B 1s and C 1s/N 1s are shown in Figure 2b. Both ratios show a significant increase toward higher polar angles. Photoelectrons emitted from the h-BN layer are more and more attenuated due to their longer pathlengths through the graphene layer at more grazing emission angles. This behavior clearly supports the g/h-BN/Cu(111) stacking order. The graphene layer thickness determined via the attenuation of the B 1s and N 1s core level intensities is 1.0 ± 0.1 ML. Attenuation factors were 0.85 for B 1s and 0.81 for N 1s for emission along the surface normal, which is in fair agreement with the attenuation for bulk graphite reduced to a thickness d of a single layer: using the relation $I(d) = I_0 e^{-(d/\lambda)}$ with d = 3.3 Å and the inelastic mean free paths λ_i of 22 Å for B 1s and 19 Å for N 1s[30] for electrons in graphite at the corresponding kinetic energies (1295.6 eV for B 1s and 1088 eV for N 1s), an attenuation for B 1s of 0.86 and for N 1s of 0.82 is found. After the graphene CVD growth the h-BN coverage as calculated with the procedure described above showed no significant change.

We have extended these core-level studies to measurements of full hemispherical intensity distributions in order to record the corresponding XPD patterns. Such data can reveal the local structural environment of typical photoemitters within a surface or a thin film sample.[31,32] The B 1s and N 1s XPD patterns shown in Figure 3a,b were recorded from the complete g/h-BN/Cu(111) stack. Both data sets show pronounced diffraction features mainly for the shallow emission angles along the rim of the plots. These features are associated with strong forward scattering enhancement along in-plane near-neighbor directions, as well as interference fringes from first-order diffraction.[32] Both diffraction patterns are in fact very similar to those from a h-BN monolayer alone.[33] This is very surprising in view of the stacking order established above: carbon atoms within the graphene layer on top of the h-BN layer should be expected to produce strong additional forward scattering peaks for lower polar angles, that is, closer to the center of the plots. However, only weaker features are observed in these regions, which can be assigned to complex interference structures from in-plane scattering of the photoemitted electrons. They can be reproduced by multiple scattering cluster (MSC) calculations from a single free-standing layer of h-BN, as is shown in Figure 3d,e.[34,35]

The absence of extra forward-scattering features in the B 1s and N 1s data could mean that the carbon layer is disordered. However, the C 1s XPD pattern displayed in Figure 3c shows a well-developed diffraction pattern, rather similar in fact to that of the N 1s signal. A multiple-scattering cluster calculation for a free-standing graphene film, shown in Figure 3f, describes this pattern quite well. From these data, we conclude that the graphene layer is well ordered with its lattice well aligned with the underlying h-BN layer. The absence of distinct forward scattering peaks in the XPD patterns from the underlying h-BN

dx.doi.org/10.1021/nl400815w | Nano Lett. 2013, 13, 2668−2675

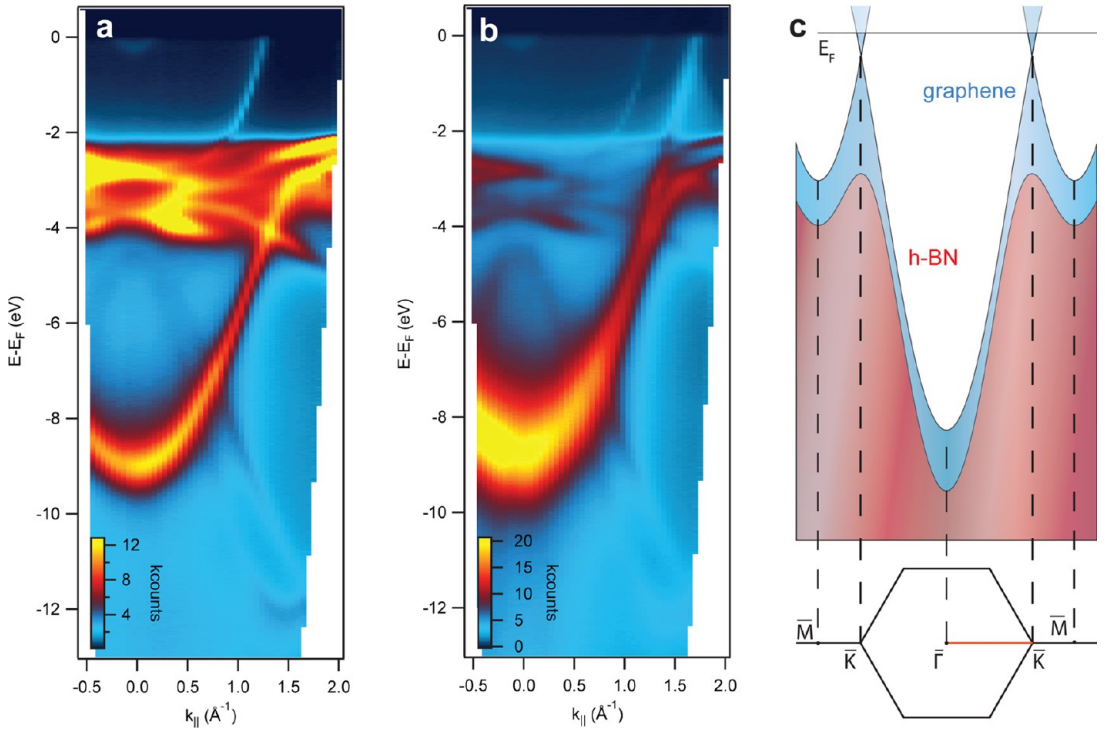

Figure 5. Band dispersion of h-BN/Cu(111) and g/h-BN/Cu(111). ARPES data of h-BN/Cu(111) (a) and of graphene on top of h-BN/Cu(111) (b), both measured along the $\bar{\Gamma}\bar{K}$ direction of the two-dimensional Brillouin zone and excited with He IIα radiation. The schematic drawing in (c) illustrates the dispersion relations of the π-bands associated with the h-BN and the graphene layers.

layer can only be rationalized by the incommensurate growth of the graphene layer, whereby the local registry of the C atoms with respect to the B and N atoms is lost.

The different lengths of the B−N bond in h-BN and the C−C bond in graphene cause a lattice mismatch of 1.6% between graphene (a_g = 2.46 Å) and h-BN (a_{BN} = 2.50 Å). When the two lattices are superimposed, moiré patterns arise with a periodicity depending on the relative orientation of the two layers.[22] STM images of the g/h-BN/Cu(111) stack are shown in Figure 4a. Flat terraces with typical dimensions of 50−100 nm are observed. On most terraces, a shallow modulation of the surface topography is found, corresponding to a regular moiré pattern with an average periodicity of 8.96 nm (see also zoom-in in Figure 4b and profile in panel c). The superposition of the well-aligned graphene and h-BN lattices results in a moiré periodicity of 15.4 nm, which corresponds to the length of 62.5 graphene unit cells. This value can be reconciled with the observed 8.96 nm periodicity by realizing that regions in this moiré pattern, where carbon atoms are situated on top of either N or B atoms or both, form a periodicity of 8.9 nm (see Figure 4d). From these data, together with the XPS/XPD results, we conclude that most of the Cu(111) surface is covered by a double layer of well aligned h-BN and graphene lattices with domain sizes of the order of 100 nm, limited by the terrace sizes of the Cu(111) substrate.

Figure 4a reveals also a peculiar type of defect on this heterolayer, taking the form of straight bands of uniform width (ca. 9 nm) and lengths of up to 150 nm with a height of ca. 0.8 nm. They could be folded graphene structures, so-called grafolds, that have recently been discussed and also experimentally observed in transferred graphene sheets.[36]

In the following, it is discussed how the structural arrangement of the g/h-BN/Cu(111) stack is reflected in the electronic bands associated with the individual sp^2-bonded layers. The band dispersion of the h-BN layer on Cu(111) along the $\bar{\Gamma}\bar{K}$ direction is shown in Figure 5a. The ARPES data were measured with He IIα excitation (photon energy $h\nu$ = 40.8 eV), where the photoelectric cross section of the π-band is much larger than that of the σ-band that dominates ARPES data taken at the He Iα photon energy.[37] The h-BN π-band is the prominent feature that disperses from a binding energy of 9.01 eV at the $\bar{\Gamma}$ point up to about 2.96 eV at the $\bar{K}$ point, mingling with the manifold of Cu 3d states[38] that shine through the boron nitride layer between 2.0 and ca. 4.5 eV. The sharp and fast dispersing band appearing between the Fermi energy and 2 eV binding energy is the sp band of the Cu substrate. The boron nitride σ-bands are vaguely visible, dispersing downward from 4 eV at the $\bar{\Gamma}$ point, where they are degenerate, to a maximum binding energy of about 12 eV at the $\bar{K}$ point. The high intensity of the π-band and the sharpness of both the π- and the σ-bands testify to the high quality of the h-BN layer.

Upon formation of the graphene layer, an additional band appears in the ARPES data (Figure 5b), while the Cu-related bands are strongly attenuated by the extra layer of carbon atoms. The new band shows linear dispersion and crosses the Fermi energy near the $\bar{K}$ point of the surface Brillouin zone, as is expected for the π-band of single-layer graphene. Also near the $\bar{K}$ point, at binding energies of around 3 eV the top of the π-band of the underlying h-BN layer is still visible and well separated from the graphene band, confirming that the h-BN layer remains intact and that its band gap persists. For lower momenta, the π-bands of the two materials appear merged into one broad band, consistent with the observations by Usachov et al.[19] on the gold-intercalated g/h-BN/Au/Ni(111) stack. At the $\bar{\Gamma}$ point, the π-band bottom appears at a binding energy of

dx.doi.org/10.1021/nl400815w | Nano Lett. 2013, 13, 2668−2675

8.71 eV. This value is about 0.5 eV lower that the one found for g/h-BN/Au/Ni(111).[19]

In the work by Usachov et al.,[19] it was argued that the role of the intercalated Au was to decouple the h-BN film from the Ni(111) surface, allowing the h-BN layer to adjust its lattice constant in order to match the one of the graphene layer as much as possible. However, our structural analysis of the g/h-BN/Cu(111) stack suggests that the two lattice constants do not need to match in order to align the two lattices. Moreover, our ARPES data, like theirs, do not show any indication for gap formation that would be expected for a lattice matched g/h-BN stack.[39]

We have therefore taken more detailed ARPES data in the vicinity of the $\bar{K}$ point (Figure 6). These measurements still

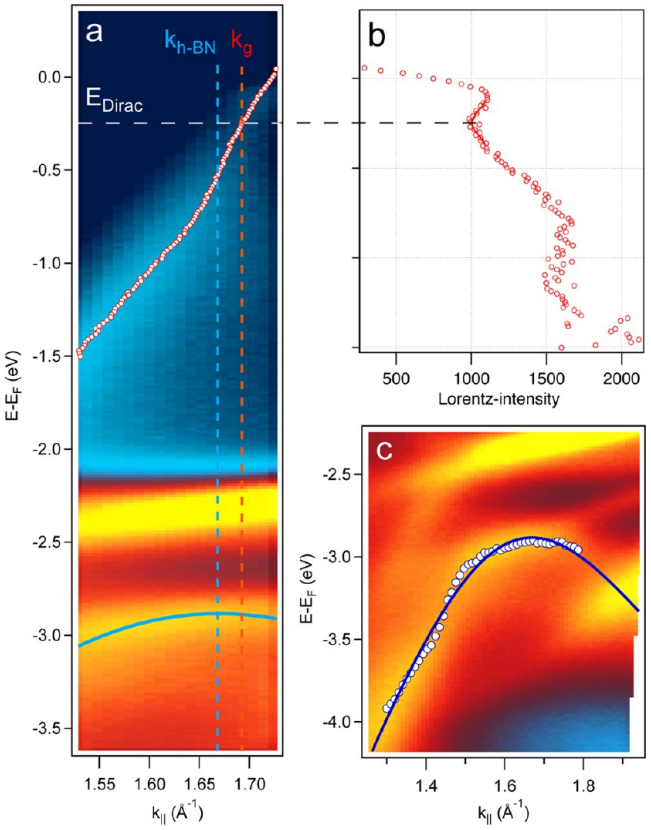

Figure 6. Lattice mismatch and energy bands. (a) He IIα excited ARPES data along $\bar{\Gamma}\bar{K}$ near the boundary of the Brillouin zone. Peak positions (dots in (a)) and intensities (b) of the graphene π-band were determined by fitting Lorentzian curves for each momentum distribution curve. The Dirac point was determined by the minimum of photoemission intensity along the π-band. The $\bar{K}$ point of h-BN is found at the maximum of the π-band. (c) The dispersion of the h-BN π-band (circles), obtained from Lorentzian fits to individual energy distribution curves, was fitted to the dispersion of a tight binding model (solid line) to precisely determine the band maximum.

show no energy gap in the graphene π-band but a distinct kink in the dispersion and an intensity minimum around the crossing of the $\bar{K}$ point. Only one branch of the Dirac cone is observed. These are well-known characteristics of a well ordered and gapless graphene layer as observed in ARPES.[40] The first two are related to many-body effects in graphene upon photoemission, the last one is a photoemission matrix element effect.

These same data can be used in order to analyze the effect of the incommensurate but well-aligned growth of the graphene layer on top of the boron nitride layer. The two different lattice constants are reflected in different periodicities also in reciprocal space, and for entirely decoupled two-dimensional electron systems this should lead to slightly different sizes of Brillouin zones. We have extracted the positions of the $\bar{K}$ points of the two layers in the following way: For the fast dispersing π-band of graphene, Lorentzian functions were fitted for individual momentum distribution curves within a range of binding energies. The positions and intensities of each fit are shown in Figure 6a,b, respectively. By comparison with the data of Bostwick et al.,[40] the Dirac point, and therefore the $\bar{K}$ point, is found where the intensity shows a local minimum, which is at a binding energy of $E_D = 0.248 \pm 0.01$ eV. Via energy dispersion curve this corresponds to a parallel momentum for the $\bar{K}$ point of $k_{\bar{K},g} = 1.693 \pm 0.005$ Å^{-1}. From this value a graphene lattice constant of $a_g = [(4\pi)/(3k_{\bar{K},g})] = 2.47 \pm 0.01$ Å^{-1} is deduced. The level of doping is comparable to the intrinsic doping of a double layer of graphene formed on SiC(0001), where $E_D = 0.29$ eV was found.[41]

The $\bar{K}$ point of the h-BN layer is located where the π-band dispersion, measured in the same ARPES data set, reaches its maximum. It was determined by fitting Lorentzian curves to individual energy distribution curves (Figure 6c), avoiding nearby Cu 3d bands. A tight binding model, where only nearest neighbor hopping was taken into account, was fitted to these data points. A dispersion relation along the $\bar{\Gamma}\bar{K}$ direction according to the equation $E(k) = E_0 - 1/2[(E_{gap}^2 + 4t^2(1 + 4\cos(ka_{BN}/2) + 4\cos^2(ka_{BN}/2))]^{1/2}$ led to a best fit where $E_0 = -0.91$ eV is the center energy of the gap, $E_{gap} = -3.94$ eV is the energy width of the gap, $a_{BN} = 2.51 \pm 0.01$ Å is the lattice constant, and $t = 2.68$ eV is the hopping parameter. The lattice constant differs by 0.5% from the one of bulk h-BN which is 2.50 Å.[12] The corresponding $\bar{K}$ point of the h-BN layer is found as $k_{\bar{K},BN} = [(4\pi)/(3a_{BN})] = 1.670 \pm 0.013$ Å^{-1}.

The mismatch observed in the photoemission data is therefore 1.4% which is close to the mismatch of two free-standing layers of 1.6%. We thus find that the two systems are electronically decoupled, except for charge transfer into the graphene sheet with each layer following its own periodicity also in reciprocal space. The emergence of new Dirac points in the band structure due to backfolding processes, involving moiré reciprocal lattice vectors, as previously seen on randomly oriented graphene flakes on h-BN by Yankowitz et al.,[42] was not observed in the present work. This might be related to the good alignment of the graphene layer with respect to the h-BN layer, leading to very long moiré periodicities. Misorientation angles smaller than 0.5° yield reciprocal lattice vectors smaller than 0.05 Å^{-1} and are therefore within the experimental linewidths measured on our samples (Figure 6a).

In conclusion, we have demonstrated a direct CVD growth of a g/h-BN stack on a Cu(111) surface. The graphene layer adopts the lattice orientation of the preformed h-BN monolayer and grows incommensurate with a lattice constant similar to that of graphite, which leads to a characteristic moiré pattern in STM images. XPS/XPD and ARPES data show that the underlying h-BN layer is not damaged during the graphene forming CVD process. The graphene π-band does not show a band gap at the $\bar{K}$ point of the Brillouin zone that has been predicted for the commensurate system,[39] where the equivalence of the two carbon atoms in the graphene lattice is lifted. The incommensurate growth effectively preserves this

dx.doi.org/10.1021/nl400815w | Nano Lett. 2013, 13, 2668−2675

equivalence over large areas thanks to the very long coherence lengths of the electrons in graphene.[43,44]

Methods. All measurements were performed at room temperature in an ultrahigh vacuum (UHV) system based on a user-modified Vacuum Generators ESCALAB 220.[45] For XPS studies, a monochromatised Al K_α X-ray source was used, providing photons with an energy of $h\nu$ = 1486.6 eV. ARPES data were measured with a microwave driven He plasma lamp equipped with a toroidal grating monochromator tuned to the He IIα line ($h\nu$ = 40.8 eV). The STM experiments were carried out in a Park Scientific VPII instrument, attached to the same UHV system, using W tips. The Cu(111) single crystal was cleaned with repetitive cycles of Ar sputtering and annealing up to 1120 K, with intermediate oxygen exposures in order to remove carbon impurities. Single layers of h-BN were prepared by CVD of borazine at a pressure of $p = 5 \times 10^{-6}$ mbar at a sample temperature of 1050 K. The thus formed layer was then usually characterized by LEED and ARPES, the latter for the appearance of the typical h-BN σ-band appearing at normal emission.[37] CVD growth of the graphene layer was done using 3-pentanone ($C_2H_5COC_2H_5$) as a precursor,[29] supplied at a pressure of p = 2.2 mbar and a substrate temperature of 1100 K, for a total exposure of about 10^9 L (1 Langmuir =1 $\times$ 10^{-6} Torr·s). Before introducing the 3-pentanone and borazine vapors to the UHV system, the stock was further purified by freezing/melting/pumping cycles.

AUTHOR INFORMATION

Corresponding Author

*E-mail: roth@physik.uzh.ch.

Notes

The authors declare no competing financial interest.

ACKNOWLEDGMENTS

The financial support from the Swiss National Science Foundation is gratefully acknowledged. Furthermore, we thank Matthias Hengsberger for fruitful discussions and Roland Stania for the programming support.

REFERENCES

(1) Geim, A.; Novoselov, K. The rise of graphene. *Nat. Mater.* **2007**, *6*, 183−191.

(2) Novoselov, K.; Geim, A.; Morozov, S.; Jiang, D. Electric field effect in atomically thin carbon films. *Science* **2004**, *306*, 666−669.

(3) Berger, C.; et al. Electronic Confinement and Coherence in Patterned Epitaxial Graphene. *Science* **2006**, *312*, 1191−1196.

(4) Martin, J.; et al. Observation of electron−hole puddles in graphene using a scanning single-electron transistor. *Nat. Phys.* **2007**, *4*, 144−148.

(5) Deshpande, A.; Bao, W.; Miao, F.; Lau, C.; LeRoy, B. Spatially resolved spectroscopy of monolayer graphene on SiO2. *Phys. Rev. B* **2009**, *79*, 205411.

(6) Emtsev, K. V.; et al. Towards wafer-size graphene layers by atmospheric pressure graphitization of silicon carbide. *Nat. Mater.* **2009**, *8*, 203−207.

(7) Li, X.; et al. Large-Area Synthesis of High-Quality and Uniform Graphene Films on Copper Foils. *Science* **2009**, *324*, 1312−1314.

(8) Gao, L.; Guest, R.; Guisinger, P. Epitaxial Graphene on Cu(111). *Nano Lett.* **2010**, *10*, 3512−3516.

(9) Bae, S.; et al. Roll-to-roll production of 30-in. graphene films for transparent electrodes. *Nat. Nanotechnol.* **2010**, *5*, 574−578.

(10) Gannett, W.; et al. Boron nitride substrates for high mobility chemical vapor deposited graphene. *Appl. Phys. Lett.* **2011**, *98*, 242105.

(11) Britnell, L.; et al. Field-Effect Tunneling Transistor Based on Vertical Graphene Heterostructures. *Science* **2012**, *335*, 947−950.

(12) Paszkowicz, W.; Pelka, J. B.; Knapp, M.; Szyszko, T.; Podsiadlo, S. Lattice parameters and anisotropic thermal expansion of hexagonal boron nitride in the 10?297.5 K temperature range. *Appl.Phys. A* **2002**, *75*, 431−435.

(13) Pozzo, M.; et al. Thermal Expansion of Supported and Freestanding Graphene: Lattice Constant versus Interatomic Distance. *Phys. Rev. Lett.* **2011**, *106*, 135501.

(14) Watanabe, K.; Taniguchi, T.; Kanda, H. Direct-bandgap properties and evidence for ultraviolet lasing of hexagonal boron nitride single crystal. *Nat. Mater.* **2004**, *3*, 404−409.

(15) Dean, C. R.; et al. Boron nitride substrates for high-quality graphene electronics. *Nat. Nanotechnol.* **2010**, *5*, 722−726.

(16) Nagashima, A.; Gamou, Y.; Terai, M.; Wakabayashi, M.; Oshima, C. Electronic states of the heteroepitaxial double-layer system. *Phys. Rev. B* **1996**, *54*, 13491.

(17) Oshima, C.; et al. A hetero-epitaxial-double-atomic-layer system of monolayer graphene/monolayer h-BN on Ni(111). *Solid State Commun.* **2000**, *116*, 37−40.

(18) Kawasaki, T.; et al. Double atomic layers of graphene/monolayer h-BN on Ni (111) studied by scanning tunneling microscopy and scanning tunneling spectroscopy. *Surf. Rev. Lett.* **2002**, *9*, 1459−1464.

(19) Usachov, D. et al. Quasifreestanding single-layer hexagonal boron nitride as a substrate for graphene synthesis. *Phys. Rev. B 82* (**2010**).

(20) Bjelkevig, C.; Mi, Z.; Xiao, J.; Dowben, P. Electronic structure of a graphene/hexagonal-BN heterostructure grown on Ru (0001) by chemical vapor deposition and atomic layer deposition: extrinsically doped graphene. *J. Phys.: Condens. Matter* **2010**, *22*, 302002.

(21) Liu, Z.; et al. Direct Growth of Graphene/Hexagonal Boron Nitride Stacked Layers. *Nano Lett.* **2011**, *11*, 2032−2037.

(22) Xue, J.; et al. Scanning tunnelling microscopy and spectroscopy of ultra-flat graphene on hexagonal boron nitride. *Nat. Mater.* **2011**, *10*, 282−285.

(23) Preobrajenski, A. B.; Vinogradov, A. S.; Mårtensson, N. Monolayer of h-BN chemisorbed on Cu(111) and Ni(111): The role of the transition metal 3d states. *Surf. Sci.* **2005**, *582*, 21−30.

(24) Joshi, S.; et al. Boron Nitride on Cu(111): An Electronically Corrugated Monolayer. *Nano Lett.* **2012**, *12*, 5821−5828.

(25) Goriachko, A.; et al. Self-Assembly of a Hexagonal Boron Nitride Nanomesh on Ru(0001). *Langmuir* **2007**, *23*, 2928−2931.

(26) Scofield, J. H. *Theoretical photoionization cross sections from 1 to 1500 keV*; Lawrence Livermore Laboratory, Report UCRL-51326: Livermore, California, United States, 1973.

(27) Werner, W. S. M. Electron transport in solids for quantitative surface analysis. *Surf. Interface Anal.* **2001**, *31*, 141−176.

(28) Mattevi, C.; Kim, H.; Chhowalla, M. A review of chemical vapour deposition of graphene on copper. *J. Mater. Chem.* **2011**, *21*, 3324.

(29) Roth, S.; Osterwalder, J.; Greber, T. Synthesis of epitaxial graphene on rhodium from 3-pentanone. *Surf. Sci.* **2011**, *605*, L17−L19.

(30) Tanuma, S. Electron Attenuation lengths. In *Surface Analysis by Auger and X-Ray Photoelectron Spectroscopy*, Briggs, D., Grant, J. T. Eds.; IM Publications: West Sussex, U.K., 2003, ch. 11.

(31) Fadley, C. S. *Syncrotron Radiation Research: Advances in Surface and Interface Science*; Plenum: New York, 1992, ch. 11.

(32) Osterwalder, J. Structural Effects in XPS and AES: Diffraction. In *Surface Analysis by Auger and X-Ray Photoelectron Spectroscopy*; Briggs, D., Grant, J. T., Eds.; IM Publications: West Sussex, U.K., 2003, ch. 20.

(33) Auwärter, W.; Kreutz, T.; Greber, T.; Osterwalder, J. XPD and STM investigation of hexagonal boron nitride on Ni (111). *Surf. Sci.* **1999**, *429*, 229−236.

(34) Matsushita, T.; Matsui, F.; Daimon, H.; Hayashi, K. Photoelectron holography with improved image reconstruction. *J. Electron Spectrosc. Relat. Phenom.* **2010**, *178−179*, 195−220.

(35) Matsui, F.; Matsushita, T.; Daimon, H. Photoelectron Diffraction and Holographic Reconstruction of Graphite. *J. Phys. Soc. Jpn.* **2012**, *81*, 114604.
(36) Kim, K.; et al. Multiply folded graphene. *Phys. Rev. B* **2011**, *83*, 245433.
(37) Grad, G.; Blaha, P.; Schwarz, K.; Auwärter, W.; Greber, T. Density functional theory investigation of the geometric and spintronic structure of h-BN/Ni(111) in view of photoemission and STM experiment. *Phys. Rev. B* **2003**, *68*, 085404.
(38) Heimann, P.; Hermanson, J.; Miosga, H.; Neddermeyer, H. D-Like Surface-State Bands on Cu(100) and Cu(111) Observed in Angle-Resolved Photoemission Spectroscopy. *Phys. Rev. B* **1979**, *20*, 3059−3066.
(39) Giovannetti, G.; Khomyakov, P. A.; Brocks, G.; Kelly, P. J.; van den Brink, J. Substrate-induced band gap in graphene on hexagonal boron nitride: Ab initio density functional calculations. *Phys. Rev. B* **2007**, *76*, 073103.
(40) Bostwick, A.; Ohta, T.; Seyller, T.; Horn, K.; Rotenberg, E. Quasiparticle dynamics in graphene. *Nat. Phys.* **2007**, *3*, 36−40.
(41) Zhou, S. Y.; et al. Substrate-induced bandgap opening in epitaxial graphene. *Nat. Mater.* **2007**, *6*, 770−775.
(42) Yankowitz, M.; et al. Emergence of superlattice Dirac points in graphene on hexagonal boron nitride. *Nat. Phys.* **2012**, *8*, 382−386.
(43) Novoselov, K. S.; et al. Two-dimensional gas of massless Dirac fermions in graphene. *Nature* **2005**, *438*, 197−200.
(44) Zhang, Y.; Tan, Y.-W.; Stormer, H. L.; Kim, P. Experimental observation of the quantum Hall effect and Berry's phase in graphene. *Nature* **2005**, *438*, 201−204.
(45) Greber, T.; et al. A photoelectron spectrometer for k-space mapping above the Fermi level. *Rev. Sci. Instrum.* **1997**, *68*, 4549.